Advances in Aerodynamics

RESEARCH

Open Access

Optimization of aero-engine combustion chambers with the assistance of Hierarchical-Kriging surrogate model based on POD downscaling method

Shuhong Tong[1,2], Yue Ma[1,2], Mingming Guo[1,2], Ye Tian[1,2*], Wenyan Song[3], Heng Wang[1], Jialing Le[1,2] and Hua Zhang[1]

*Correspondence:
tianye@cardc.cn

[1] Southwest University of Science and Technology, Mianyang 621000, China
[2] China Aerodynamics Research and Development Center, Mianyang 621000, China
[3] Northwestern Polytechnical University, Xi'an 710072, China

Abstract

In view of the long calculation cycle, high processing test and cost of the traditional aero-engine combustion chamber design process, which restricts the engine optimization design cycle, this paper innovatively proposes a surrogate model for the performance of aero-engine combustion chambers based on the POD-Hierarchical-Kriging method. Through experiments, the predicted results of the POD-Hierarchical-Kriging model are compared and analyzed with the calculated results of the one-dimensional program, and the root mean square error of the predicted values of combustion efficiency and total pressure loss is 0.0064% and 0.1995%, respectively. The accuracy of the POD-Hierarchical-Kriging model is compared with the cubic polynomial model, the basic Kriging model and the Hierarchical-Kriging model. It verifies the feasibility and accuracy of the POD-Hierarchical-Kriging model for the prediction of performance of aero-engine combustion chambers. The global sensitivity analysis method is applied to obtain the influence effect of design variables on the performance. Then, a multi-objective optimization method based on the NSGA-II algorithm is studied, and finally the optimal set of Pareto solutions is obtained and analyzed, which can be used to guide the optimal design of aero-engine combustion chambers and accelerate the progress of aero-engine development.

Keywords: Aero-engine combustion chamber, Surrogate model, POD-Hierarchical-Kriging, Multi-objective optimization

1 Introduction

With the development and innovation of aero-engine technology by using a few novel strategies [1], reducing the engine design cycle and calculation time has become an important part of current research. As one of the three core components of an aero-engine, the engine combustion chamber has higher requirements for design development cycle and design results. The current combustion chamber design basically relies on CFD numerical simulations or wind tunnel tests for calculation and evaluation.

The high complexity of models and methods leads to long computational cycles and still large computational costs. In recent years, reducing the computational cost and improving the optimization efficiency by using surrogate models to approximate the target quantity have been widely studied by scholars. It mainly adopts a data-driven modeling approach for fit, regression, and feature learning based on a sample database composed of selected design variables and corresponding numerical calculations or real test results. Surrogate models that can highly approximate the real mathematical model are constructed, and the corresponding output parameters can be quickly and accurately obtained for the input parameters of the surrogate model, which can replace the complex and time-consuming calculation and analysis in the design process. The commonly used surrogate models in current research include polynomial response surfaces, moving least squares, radial basis functions, artificial neural networks, support vector machines, Kriging (Gaussian regression process), etc.

At present, with the development of neural networks, many scholars have applied neural networks to build surrogate models suitable for engine optimization design. M. Taghavi et al. [2] used three popular structures – nonlinear autoregressive network with exogenous inputs (NARXNET), multilayer perceptron (MLP) and radial basis function (RBF) to build a multi-input single-output surrogate model to predict the start of the combustion (SOC) of homogeneous charge compression ignition (HCCI) engine operation. Caterina Poggi et al. [3] developed an artificial neural network (ANN) surrogate model suitable for simulating aerodynamic performance and acoustic emission, avoiding the need for computationally costly CFD/CAA predictions. Although the ANN-based surrogate model can promote the optimization of engine design, the establishment of an artificial neural network surrogate model requires a large number of samples and a lot of time for model training. Therefore, in order to establish the surrogate model more quickly with fewer data samples, the Kriging surrogate model and the polynomial response surfaces surrogate model have more advantages in establishing the engine surrogate model. Hideaki Ogawa [4] combined computational fluid dynamics and evolutionary algorithms to optimize the multi-objective fuel injection at Mach 5.7 cross-flow, which is after initial compression of Mach 7.6 inlet, with the assistance of various surrogate modeling including polynomial and Kriging. Fernando Tejero et al. [5, 6] designed and studied the non-axisymmetric aero-engine nacelle based on the Kriging surrogate model method. A series of surrogate-based adaptation methods are studied in order to reduce the computational cost.

However, the basic Kriging surrogate model has high requirements on the confidence of sample data, so some researchers have proposed some new surrogate models based on the basic Kriging model and applied them to the optimization design of engines. ZH Han et al. [7] proposed the Hierarchical-Kriging model, using a sampled Kriging model with a low fidelity function as the model trend. A more accurate surrogate model of the high fidelity function is obtained by mapping the variation of the low fidelity data to the high fidelity data. It is also used to model the aerodynamic data of RAE2822 airfoil and industrial transport aircraft structures with efficiency, accuracy and robustness. Du et al. [8] applied the Hierarchical-Kriging to optimize the structural dynamics of rocket engines, constructed the relationship between the

design variables of engine structural parameters and modal frequency characteristics, and used it to facilitate engine optimization design, achieving good accuracy.

In recent years, some researchers have established some surrogate models for the aero-engine combustor to assist the optimization design of the combustor, but there exist still few relevant studies. Maotao Yang et al. [9] used the Kriging surrogate model to predict the combustion efficiency and total pressure loss of the combustion chamber and compared it with the ANN model to verify that the use of the Kriging surrogate model can shorten the engine combustion chamber design cycle. Yue Ma et al. [10] used a cubic polynomial surrogate model to predict the performance of combustion chambers. Based on this, a multi-objective optimization of the combustion chamber performance is carried out using the particle swarm optimization (PSO) algorithm. The surrogate model is proved to be useful for guiding the combustion chamber design. All their studies have verified that the use of surrogate models can promote the optimization design of aero-engine combustors, but the surrogate models they used are all basic surrogate models, which also have high requirements on the confidence of sample data.

Based on the analysis of the above research status, the application of surrogate models to assist engine optimization design has achieved good development, but most of the above studies ignore the possible information redundancy under the optimization of multiple design variables in the process of establishing the surrogate model. This information redundancy adds unnecessary computing costs. Aero-engine combustor has the characteristics of large variation in working conditions, significant nonlinearity and harsh working environment, so the application of surrogate model-assisted engine optimization design of aero-engine combustors has very good development potential. However, in the above studies, little work has been carried out on the aeroengine combustion chamber. Maotao Yang and Yue Ma respectively used the Kriging surrogate model and the cubic polynomial surrogate model to study the optimal design of aeroengine combustion chambers. However, both of these two surrogate models have high requirements on the confidence of training samples. Therefore, in order to make up for the shortcomings of the above surrogate models, a new surrogate model needs to be designed, which will not be affected by information redundancy in the design variable space during the design process, and can use the training samples with low confidence to establish a high-precision surrogate model.

Under the above requirements, this paper takes an aero-engine combustion chamber as the research object, and creatively applies the POD-Hierarchical-Kriging method to establish a surrogate model of combustion performance. Firstly, different incoming flow conditions and main design parameters of the combustion chamber are selected as design variables. The sample collection in the input parameter space is completed by using the Latin hypercube sampling method. A numerical simulation program designed by Northwestern Polytechnical University is applied to pre-process the data and calculate the output values of combustion performance including combustion efficiency and total pressure loss. Then the samples are downscaled and reconstructed based on the POD algorithm, and the downscaled and reconstructed data are used as training datasets. Based on the Hierarchical-Kriging method, a surrogate model is developed to characterize the mapping relationship between the input and output performance parameters of the original complex model to simplify the complex and time-consuming

computational process. Finally, the constructed data set is used to complete the training of the model, and the test data is used for verification. A global sensitivity analysis method based on variance is applied to rank the magnitude of design variables affecting the combustion performance. Based on the POD-Hierarchical-Kriging model, a Pareto optimal solution set is obtained by the NSGA-II multi-objective optimization algorithm, laying the foundation for the optimal design of aero-engine combustion chambers.

In Section 2 of this paper, the concentric graded combustion chamber model is introduced. Section 3 carries out the theoretical derivation of the POD algorithm, the basic Kriging and Hierarchical-Kriging surrogate models, and the theory of the NSGA-II algorithm. In Section 4, experiments are carried out, including surrogate model test prediction and error comparison analysis of various surrogate models, global sensitivity analysis, as well as multi-objective optimization based on the NSGA-II algorithm. The Pareto solution set obtained from optimization is analyzed. Section 5 provides a summary.

2 Combustion chamber model and data acquisition

2.1 Reliability verification of high performance 1D design method

In order to quickly complete the calculation of combustor parameters, the one-dimensional calculation method of aero-engine combustor is studied jointly with Kazan Aviation University, and a set of one-dimensional calculation program of aero-engine combustor model is developed. Taking a dual swirl combustor as the object, the calculated state is a full pressure state, in which the total inlet temperature is 861.49 K, the inlet pressure is 33.4 atm, the air flow is 54.38 kg/s, and the total oil–gas ratio in the combustor is 0.026. The reliability of the three-dimensional numerical calculation is verified by comparing the experimental results with the three-dimensional numerical calculation results of the dual swirl combustor. After that, two different one-dimensional calculation models (Case 1 and Case 2) are adopted. In the one-dimensional design program, different calculation models, correlation expressions or constants can be selected according to the calculation needs. The calculation methods are shown in Table 1. The consistency of the one-dimensional calculation method is verified by comparing the one-dimensional calculation results with the three-dimensional numerical results verified by reliability.

In the comparison between the three-dimensional calculation of the combustion chamber and the test, the PIV test measured the velocity field through the center section of the full hole of the main combustion hole. The PIV observation area is shown in Fig. 1. The velocity field before and after the main combustion hole is measured by PIV, and the measured results are processed dimensionlessly. Figures 2, 3 and 4 show the comparison cloud images between the calculated results of three-dimensional velocity field and the measured results of PIV test. By comparing with the PIV measurement results, it can be seen that the velocity field distribution trend of the 3D numerical simulation cloud image is basically consistent with the experimental measurement results, and the error is within a reasonable range, which indicates that the 3D numerical simulation can reflect the changes and characteristics of the actual flow field to a certain extent.

Table 1 Model selection of two one-dimensional calculation methods

Selection	Calculation method	
	Case 1	Case 2
Diffuser section 1–2 section calculation method	Flow tube method	Flow tube method
Diffuser section 2–4 section calculation method	Empirical method + Mixed method	Mixed method + Mixed method
Jet mixing model	Quality loss	Equivalent blending
Penetrating flux mixing constant	1	1
Wall jet mixing constant	0.1	0.2
Correlations used to calculate emissivity	Reeves on Distilled Fuel Correlation (non-luminous flame)	NREC 1964 correlation (glowing flame)
Radiation dimension	One-dimensional	One-dimensional
Whether to consider radiation heat transfer between walls	No	No
Whether to use wall cooling	Yes	Yes
Whether to consider the longitudinal heat conduction between walls	No	No
Whether to conduct heat through the annular cavity air	Yes	No

Then, the one-dimensional calculation methods Case 1, Case 2 and CFD three-dimensional calculation are used to obtain the comparison for the air flow rate accumulated along the axial direction, as shown in Table 2. There are a row of main combustion holes and mixing holes respectively on each wall of the flame cylinder. The main combustion hole cross section is cut off along the axial direction at the main combustion hole, and the mixing hole cross section is cut off along the axial direction at the mixing hole. It can be seen that the results of Case 1 calculation are closer to those of CFD three-dimensional calculation, and the inlet air volume in the main combustion zone is only slightly less than that of Case 2 calculation.

Table 3 is a comparison of the performance parameters obtained by the one-dimensional calculation methods Case 1, Case 2 and CFD three-dimensional calculation. It can be seen from Table 3 that the calculation results meet the requirements of the combustion chamber performance parameters.

Based on the comparison and analysis of the flow parameters and performance parameters of the combustion chamber mentioned above, it can be seen that the one-dimensional calculation method adopted is in good agreement with the three-dimensional calculation. It is proved that the one-dimensional calculation method can calculate the performance parameters of the combustion chamber well, and the calculation results are accurate and feasible. A more detailed description of the method can be found in reference [11].

2.2 High performance combustion chamber design for aero engine

The object of this paper is a type of concentric graded combustion chamber. The design conditions met by this combustion chamber are shown in Table 4, and its structure schematic is shown in Fig. 5. According to the design requirements, the overall structural parameters and flow distribution of the combustion chamber are

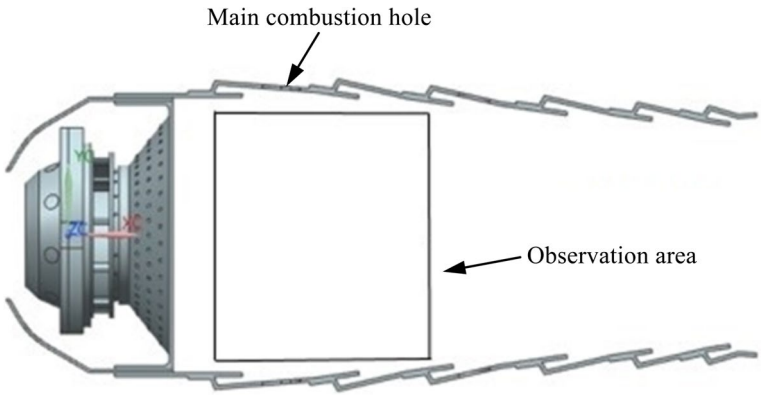

Fig. 1 PIV observation area

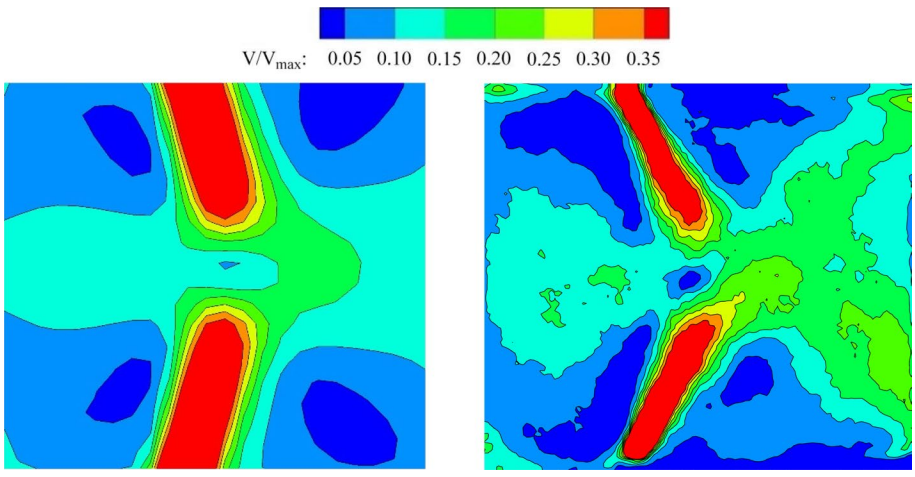

Fig. 2 Comparison of numerical simulation and experimental results of velocity distribution in central section of main combustion hole in the dual swirl combustor

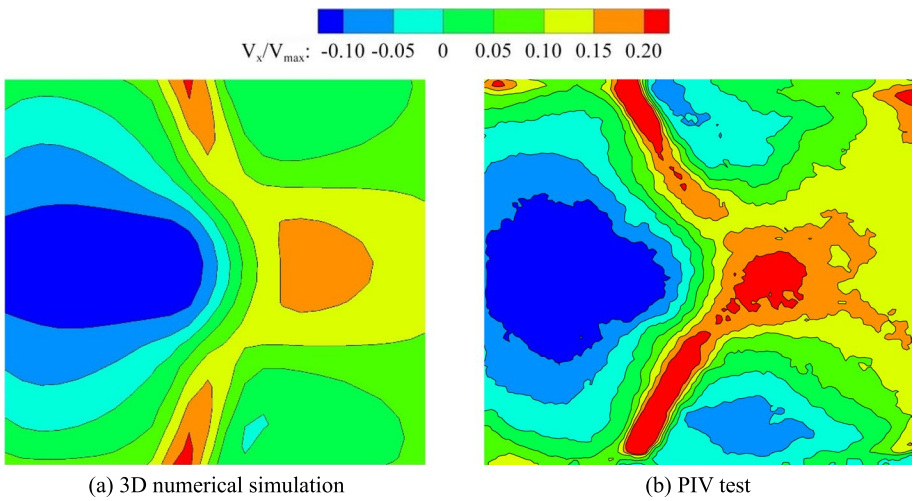

Fig. 3 Comparison of numerical simulation and experimental results of axial velocity distribution in central section of main combustion hole in the dual swirl combustor

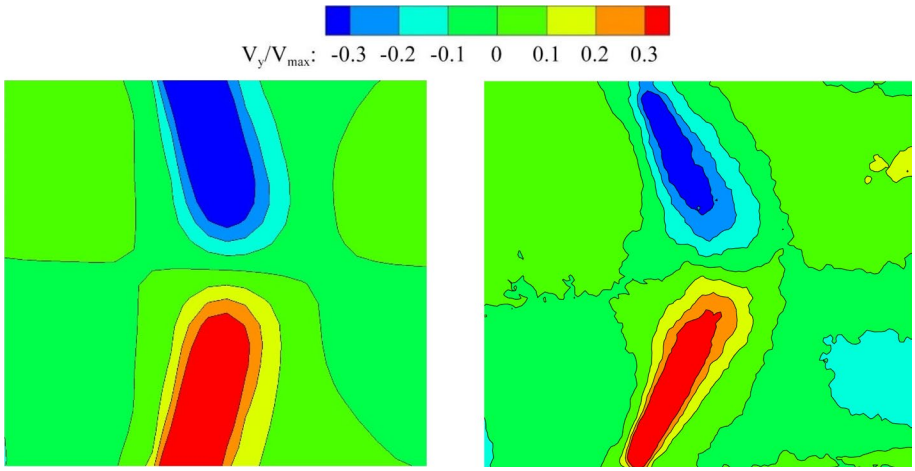

(a) 3D numerical simulation (b) PIV test

Fig. 4 Comparison of numerical simulation and experimental results of radial velocity distribution in central section of main combustion hole in the dual swirl combustor

Table 2 Comparison of cross-sectional flow distribution ratios between the main combustion hole and the mixing hole in the dual swirl combustor

Calculation method	Main combustion hole cross section	Mixing hole cross section
1D calculation (Case 1)	0.488	0.809
1D calculation (Case 2)	0.490	0.804
CFD 3D calculation	0.476	0.848

Table 3 Comparison of combustion chamber performance parameters

Performance parameters	Case 1	Case 2	CFD 3D calculation results
Combustion efficiency	0.9994	0.9994	0.9974
Total pressure recovery	0.9601	0.9565	0.9604
OTDF	0.2053	0.2054	0.261

calculated, and on this basis, the design and calculation of each component of the combustion chamber are carried out. Finally, the preliminary design scheme of the combustion chamber is obtained. Through numerical simulation and test verification, it has been verified that this structure can meet certain performance index requirements. For more detailed design parameters, refer to literature [12].

Based on the concentric graded combustion chamber model, the surrogate model construction is carried out according to the calculation results of the one-dimensional program of the self-designed aero-engine combustion chamber model. Combustion efficiency $\eta(\%)$ and total pressure loss $\Delta p(\%)$ are selected as the target parameters. Design parameters are selected as total inlet temperature T_t(K), total inlet pressure P_t (kPa), inlet flow S_t(kg/s), oil–gas ratio R_{og}, number of main combustion holes (single

Table 4 High temperature rise combustor design requirements

Parameters	Design status	Slow state
Total inlet temperature (K)	850	492.9
Oil–gas ratio	0.0430	0.0106
Combustion efficiency	> 99%	> 98%
Total pressure loss	< 6%	< 7%
Overall temperature distribution factor	< 0.20	-
Radial temperature distribution factor	< 0.12	-

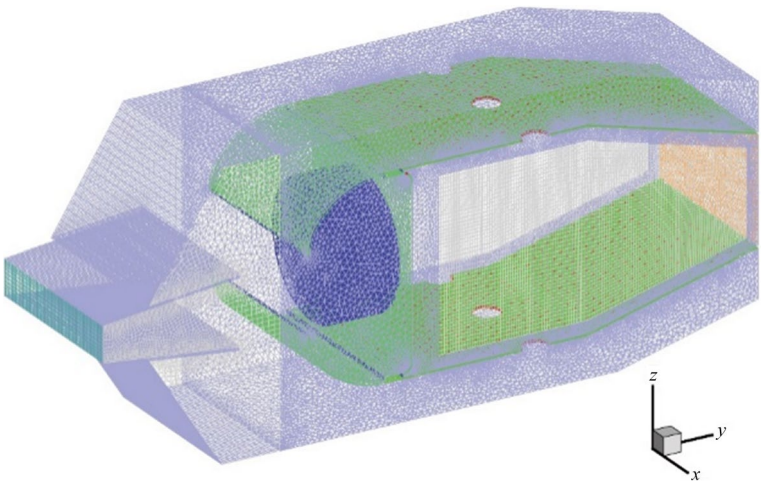

Fig. 5 Overall grid structure of combustion chamber

head and single wall) N_m(PCS), size of main combustion holes D_m(mm), number of cooling holes in each row N_c(PCS) and size of cooling holes D_c(mm). The design variables are detailed in Table 5.

The combustor surrogate model design algorithm process mainly includes the following parts. First, Latin hypercube sampling is carried out in the 8-variable space to obtain sample data of input parameters. Then, the self-designed one-dimensional program of aero-engine combustion chamber model is used for calculation, and the corresponding combustion efficiency and total pressure loss of sample parameters are obtained. After data preprocessing, the sample data set is constructed and completed.

Table 5 Design variables

Variable symbols	Variable name	Range of changes
T_t/K	Total inlet temperature	427.55 – 1070.33
P_t/kPa	Total inlet pressure	500 – 3200
S_t/kg$_*$s^{-1}	Total inlet flow	19.01 – 82.398
R_{og}	Oil–gas ratio	0.0106 – 0.0430
N_m/PCS	Number of main combustion holes	2 – 4
D_m/mm	Size of main combustion holes	12.1 – 16.8
N_c/PCS	Number of cooling holes per row	10 – 20
D_c/mm	Cooling hole size	0.5 – 1.5

Then, mapping relationships between eight input parameters and two output parameters ($\eta/\Delta p$) are established based on the POD-Hierarchical-Kriging model to replace the complex model among variables, that is, the surrogate model for aeroengine combustion chamber is constructed. Finally, based on the NSGA-II optimization algorithm and the surrogate model, the design parameters are optimized and the optimal configuration is obtained.

3 Method

3.1 Design of POD-Hierarchical-Kriging combustion performance surrogate model

The POD-Hierarchical-Kriging algorithm model is mainly based on the Kriging model. The Kriging model regards the unknown function as the concrete realization of a static stochastic process, including regression part and correlation part, among which the correlation part can be regarded as the realization of random Gaussian process, and has a good fitting effect for problems with a high degree of nonlinearity. The Kriging model is based on the dynamic construction of sample information at known points and has both global and local statistical characteristics. The POD algorithm [13–15] is used to downscale and reconstruct the original samples, reduce the sample computational loss, extract the core information, and filter out the marginal information. The data processed by the POD algorithm is used as the sample input for the Hierarchical-Kriging model. The above whole constitutes the POD-Hierarchical-Kriging algorithm model.

3.1.1 POD method

The core of the POD method is to find a set of "optimal" orthogonal bases $\{\boldsymbol{U}_1, \boldsymbol{U}_2, \boldsymbol{U}_3, \cdots, \boldsymbol{U}_n\}$ of the n-dimensional field space $\{\boldsymbol{x}_n \in \Omega\}$. Assuming that $\boldsymbol{x}_n$ can be approximated by a number of orthogonal bases, then $\boldsymbol{x}_n$ can be approximated by this set of "optimal" orthogonal bases $\{\boldsymbol{U}_1, \boldsymbol{U}_2, \boldsymbol{U}_3, \cdots, \boldsymbol{U}_n\}$:

$$\boldsymbol{x}_n = \sum_{i=1}^{n} \alpha_i \boldsymbol{U}_i. \tag{1}$$

Where $\boldsymbol{U}_i$ is the eigenvector or basis vector of $\boldsymbol{x}_n$; α_i is the correlation coefficient of $\boldsymbol{U}_i$. If the dimension of the orthogonal space composed of "optimal" orthogonal bases is smaller than that of the original space, the above approximation process can be described as a downscaling of the sample space, followed by an approximate reconstruction of the sample, then:

$$\boldsymbol{x}_n = \sum_{i=1}^{r} \alpha_i \boldsymbol{U}_i, (r < n). \tag{2}$$

Therefore, the centralization of the sample data is performed. Then the new centralized sample data set is obtained:

$$\begin{aligned} \widetilde{\boldsymbol{X}} &= \left\{\widetilde{\boldsymbol{x}}_1, \widetilde{\boldsymbol{x}}_2, \widetilde{\boldsymbol{x}}_3, \cdots, \widetilde{\boldsymbol{x}}_n\right\} \\ &= \{\boldsymbol{x}_1 - \overline{\boldsymbol{x}_1}, \boldsymbol{x}_2 - \overline{\boldsymbol{x}_2}, \boldsymbol{x}_3 - \overline{\boldsymbol{x}_3}, \cdots, \boldsymbol{x}_n - \overline{\boldsymbol{x}_n}\}, \end{aligned} \tag{3}$$

followed by SVD (singular value decomposition):

$$\widetilde{\boldsymbol{X}} = \boldsymbol{U}\boldsymbol{\Sigma}\boldsymbol{V}^T. \tag{4}$$

For the value of r, r should be less than n to reduce the scale of the feature vector space, but it should approximate the original data space as accurately as possible. The selection of r can be determined in the following ways:

$$I = \sum_{i=1}^{r} (\lambda_i)^2 / \sum_{i=1}^{n} (\lambda_i)^2. \tag{5}$$

I is the energy information capacity or energy. The closer I is to 1, the more complete the original information contained in the feature vector space is and the closer it is to the original function space. It is usually considered that I is greater than 95%. Where λ is the eigenvalue of the covariance matrix $\widetilde{\boldsymbol{X}}$ arranged from the largest to the smallest, satisfying $\lambda_1 > \lambda_2 > \cdots > \lambda_n$. Then the final POD model is:

$$\boldsymbol{X}_{RE} = \overline{\boldsymbol{X}} + \sum_{i=1}^{r} \alpha_i \boldsymbol{U}_i. \tag{6}$$

3.1.2 Basic Kriging model

The Kriging model is an unbiased estimation model. It has the characteristics of local estimation and is a good fit for problems with a high degree of nonlinearity. The following is a reference to the derivation process of Kriging method theory [16, 17]. In the analysis of regression model, the model assumes that the real relationship between the response value of the system and the independent variable can be expressed in the following form:

$$\boldsymbol{y}(\boldsymbol{x}) = \boldsymbol{f}(\boldsymbol{x})^T \boldsymbol{\beta} + \boldsymbol{z}(\boldsymbol{x}). \tag{7}$$

Where $\boldsymbol{x}$ is the input parameter; $\boldsymbol{f}(\boldsymbol{x}) = \left[f_1(\boldsymbol{x}), f_2(\boldsymbol{x}), \cdots, f_p(\boldsymbol{x})\right]^T$; $\boldsymbol{\beta}$ is the regression constant, expressed as $\boldsymbol{\beta} = \left[\beta_1, \beta_2, \ldots, \beta_p\right]^T$; p is the number of polynomial terms, and the magnitude depends on the form of the polynomial; $y(\boldsymbol{x})$ is the predicted value of combustion efficiency $\eta(\%)$ or total pressure loss $\Delta p(\%)$, $\boldsymbol{y}(\boldsymbol{x}) = [\eta, \Delta p]$; $\boldsymbol{z}(\boldsymbol{x})$ is a random process, which has the following statistical properties:

$$\begin{cases} E[\boldsymbol{z}(\boldsymbol{x})] = 0, \\ Var[\boldsymbol{z}(\boldsymbol{x})] = \sigma^2, \\ E[\boldsymbol{z}(\boldsymbol{x}^i), \boldsymbol{z}(\boldsymbol{x})] = \sigma^2 \boldsymbol{R}. \end{cases} \tag{8}$$

Where,

$$\boldsymbol{R} = \begin{bmatrix} \rho_{11} & \rho_{12} & \cdots & \rho_{1m} \\ \rho_{21} & \rho_{22} & \cdots & \rho_{2m} \\ \vdots & \vdots & \ddots & \vdots \\ \rho_{m1} & \rho_{m2} & \cdots & \rho_{mm} \end{bmatrix}, \tag{9}$$

and $\boldsymbol{R}$ is "correlation matrix"; ρ_{ij} is the correlation function value, representing the correlation between the i^{th} sample point and the j^{th} sample point; m is the size of the sample. The correlation function is artificially assumed, and the Gaussian function is commonly used. In this experiment, the Gaussian function is used as the correlation function, and the specific form is as follows:

$$\rho_{ij} = \exp\left(-\sum_{h=1}^{n} \theta_h \left| x_h^i - x_h^j \right|^2\right), i, j = 1, 2, \ldots, m. \tag{10}$$

Where the unknown parameter $\boldsymbol{\theta} = [\theta_1, \theta_2, \ldots, \theta_n]$, the dimension n is the same size as the dimension of the sample point. x_h^i is the h^{th} variable of the i^{th} sample and can be expressed as any of the input parameters.

A prediction model formula (11) is given to approximate formula (7):

$$\widehat{\boldsymbol{y}}(\boldsymbol{x}) = \boldsymbol{c}^T(\boldsymbol{x})\boldsymbol{Y}. \tag{11}$$

Where $\boldsymbol{Y} = [y_1, y_2, \ldots, y_m]^T$, and $\boldsymbol{Y}$ is the known sample response vector; $\boldsymbol{c} = [c_1(\boldsymbol{x}), c_2(\boldsymbol{x}), \ldots, c_m(\boldsymbol{x})]^T$, and c_i is related to a single sample point $\boldsymbol{x}$. When the given sample points $\boldsymbol{x}$ are different, the resulting c_i is different.

The prediction error of the model is:

$$\widehat{\boldsymbol{y}}(\boldsymbol{x}) - \boldsymbol{y}(\boldsymbol{x}) = \boldsymbol{c}^T\boldsymbol{z} - \boldsymbol{z} + \left(\boldsymbol{F}^T\boldsymbol{c} - \boldsymbol{f}(\boldsymbol{x})\right)^T\boldsymbol{\beta}. \tag{12}$$

Where $\boldsymbol{z} = [\boldsymbol{z}(\boldsymbol{x}_1), \boldsymbol{z}(\boldsymbol{x}_2), \cdots, \boldsymbol{z}(\boldsymbol{x}_m)]^T$, and $\boldsymbol{F} = \left[\boldsymbol{f}^T(\boldsymbol{x}_1), \boldsymbol{f}^T(\boldsymbol{x}_2), \ldots, \boldsymbol{f}^T(\boldsymbol{x}_m)\right]^T$. Considering that $\widehat{\boldsymbol{y}}(\boldsymbol{x})$ is the optimal linear unbiased estimate of $\boldsymbol{y}(\boldsymbol{x})$, Eq. (13) is obtained from the unbiased estimate, and Eq. (14) is obtained from the minimum mean square error.

$$\boldsymbol{F}^T\boldsymbol{c} = \boldsymbol{f}(\boldsymbol{x}). \tag{13}$$

$$MSE = \boldsymbol{\sigma}^2\left(1 + \boldsymbol{c}^T\boldsymbol{R}\boldsymbol{c} - 2\boldsymbol{c}^T\boldsymbol{r}\right). \tag{14}$$

Where $\boldsymbol{r}$ is the correlation vector composed of the correlation function between the point $\boldsymbol{x}$ to be predicted and the original sample set. By constructing the Lagrangian function, the response model expression can be obtained:

$$\widehat{\boldsymbol{y}}(\boldsymbol{x}) = \boldsymbol{f}(\boldsymbol{x})^T\boldsymbol{\beta}^* + \boldsymbol{r}(\boldsymbol{x})^T\boldsymbol{\gamma}^*. \tag{15}$$

Where, $\boldsymbol{\beta}^* = \left(\boldsymbol{F}^T\boldsymbol{R}^{-1}\boldsymbol{F}\right)^{-1}\boldsymbol{F}^T\boldsymbol{R}^{-1}\boldsymbol{Y}$, and $\boldsymbol{\gamma}^* = \boldsymbol{R}^{-1}\left(\boldsymbol{Y} - \boldsymbol{F}^T\boldsymbol{\beta}^*\right)$. It can be seen that $\boldsymbol{F}$ and $\boldsymbol{Y}$ can be obtained from the given sample, and $\boldsymbol{R}$ contains only the parameter $\boldsymbol{\theta}$. $\boldsymbol{\beta}^*$, $\boldsymbol{\gamma}^*$, and $\boldsymbol{r}(\boldsymbol{x})$ can be obtained by finding the unknown parameter $\boldsymbol{\theta}$.

Since each sample point is not independent, the joint probability density is:

$$L\left(\boldsymbol{\beta}, \boldsymbol{\sigma}^2, \boldsymbol{\theta}\right) = \frac{1}{(2\pi)^{m/2}\left(\boldsymbol{\sigma}^2\right)^{m/2}|\boldsymbol{R}|^{1/2}} \exp\left[-\frac{1}{2\boldsymbol{\sigma}^2}\left(\boldsymbol{Y} - \boldsymbol{F}^{\mathrm{T}}\boldsymbol{\beta}\right)^T\boldsymbol{R}^{-1}\left(\boldsymbol{Y} - \boldsymbol{F}^{\mathrm{T}}\boldsymbol{\beta}\right)\right]. \tag{16}$$

Taking the logarithm:

$$\ln L \approx -\frac{1}{2}\left(m\ln\widehat{\boldsymbol{\sigma}}^2 + \ln(|\boldsymbol{R}(\boldsymbol{\theta})|)\right), \tag{17}$$

where $\ln L$ only contains the parameter $\boldsymbol{\theta}$, and the parameter training is transformed into the solution of a nonlinear optimization problem, which in turn yields $\boldsymbol{R}$. Then $\boldsymbol{\beta}^*$, $\boldsymbol{\gamma}^*$, and $\boldsymbol{r}(\boldsymbol{x})$ are similarly available, so the final model is determined.

3.1.3 Hierarchical-Kriging model

The difference between the Hierarchical-Kriging and the basic Kriging is that the Hierarchical-Kriging adopts a multi-layer basic Kriging structure [7, 16]. The Hierarchical-Kriging allows the output of the first layer to be the global approximate reference of the second layer, the second layer to be the global approximate reference of the third layer, and so on. The Hierarchical-Kriging has a very great advantage in practical applications in making full use of the sample information [16, 17]. The basic Kriging is too sensitive to the noise of training samples and requires high reliability of training samples, while it is easy to overfit training samples with low reliability. However, the Hierarchical-Kriging adopts a hierarchical strategy, training the first layer with samples of low confidence and the second layer with samples of high confidence, so as to fully explore the potential of training samples. Take the Hierarchical-Kriging with two layers as an example:

To construct the two-layer Kriging, the first layer Kriging should be constructed with low confidence training sample points.

$$y_{1\mathrm{f}}(\boldsymbol{x}) = \beta_{1\mathrm{f}} + z_{1\mathrm{f}}(\boldsymbol{x}). \tag{18}$$

The polynomial in the model of the first layer is a constant, because the reliability of the training sample is low, and it is easy to fit the noise with the polynomial of higher order, resulting in the decline of the prediction accuracy of the final model.

$$\widehat{y}_{1\mathrm{f}}(\boldsymbol{x}) = \beta_{1\mathrm{f}} + \boldsymbol{r}_{1\mathrm{f}}^{T}(\boldsymbol{x})\mathbf{R}_{1\mathrm{f}}^{-1}\left(\mathbf{y}_{1\mathrm{f}} - \beta_{1\mathrm{f}}1\right). \tag{19}$$

Where $\beta_{1\mathrm{f}} = \left(1^{T}\mathbf{R}_{1\mathrm{f}}^{-1}1\right)^{-1}1^{T}\mathbf{R}_{1\mathrm{f}}^{-1}\mathbf{y}_{1\mathrm{f}}$, $\mathbf{R}_{1\mathrm{f}} \in \mathbb{R}^{n_{1\mathrm{f}}\times n_{1\mathrm{f}}}$, $1 \in \mathbb{R}^{n_{1\mathrm{f}}}$, $\boldsymbol{r}_{1\mathrm{f}} \in \mathbb{R}^{n_{1\mathrm{f}}}$. This is the result of training through the first layer of samples.

The second layer structure is constructed on the basis of the first layer, and the high reliability sample points are used to train the second layer.

$$y_{2\mathrm{f}}(\boldsymbol{x}) = \beta\widehat{y}_{1\mathrm{f}}(\boldsymbol{x}) + z(\boldsymbol{x}). \tag{20}$$

Using the same derivation as the first level, it can be derived that:

$$\widehat{y}_{2\mathrm{f}}(\boldsymbol{x}) = \beta\widehat{y}_{1\mathrm{f}}(\boldsymbol{x}) + \boldsymbol{r}_{2\mathrm{f}}^{T}(\boldsymbol{x})\mathbf{R}_{2\mathrm{f}}^{-1}\left(\mathbf{y}_{2\mathrm{f}} - \beta\boldsymbol{F}\right). \tag{21}$$

Where $\boldsymbol{F} = [\widehat{y}_{1\mathrm{f}}(\boldsymbol{x}_1), \ldots, \widehat{y}_{1\mathrm{f}}(\boldsymbol{x}_m)]^{T}$; $\mathbf{R}_{2\mathrm{f}}$ and $\boldsymbol{r}_{2\mathrm{f}}$ are both correlation matrices and correlation vectors composed with high confidence sample points (in the same specific form as the basic Kriging); $\mathbf{y}_{2\mathrm{f}}$ is a vector composed of responses from sample points; $\beta = \left(\boldsymbol{F}^{T}{\mathbf{R}_{2\mathrm{f}}}^{-1}\boldsymbol{F}\right)^{-1}\boldsymbol{F}^{T}{\mathbf{R}_{2\mathrm{f}}}^{-1}\mathbf{y}_{2\mathrm{f}}$.

3.2 NSGA-II multi-objective optimization design

Genetic algorithm is widely used in aero-engine design [18, 19]. NSGA-II is a multi-objective optimization algorithm based on the optimal Pareto solution. It has the characteristic of low complexity, and uses the elite population strategy and the degree of crowding comparison operator. The key steps of NSGA-II include fast non-dominated sorting, calculation of congestion, elite reservation policy and tournament selection.

The target parameters involved in the engine combustion chamber design are combustion efficiency η and total pressure loss Δp, where the combustion efficiency η should be

as large as possible to ensure $\eta \geq 99\%$, and the total pressure loss Δp should be as small as possible to ensure $\Delta p \leq 4\%$. To meet the constraints, the overall temperature distribution factor (OTDF) should be less than 0.2.

According to the multi-objective minimum optimization model, the optimization model can be described as:

$$obj.\begin{cases} max - \eta(T_t, P_t, S_t, R_{og}, N_m, D_m, N_c, D_c), \\ min\ \Delta p(T_t, P_t, S_t, R_{og}, N_m, D_m, N_c, D_c), \end{cases} \tag{22}$$

$$constraint : OTDF \in [0, 0.20], \tag{23}$$

$$s.t.\begin{cases} T_t \in [427.55,1070.33], \\ P_t \in [500,3200], \\ S_t \in [19.01,82.398], \\ R_{og} \in [0.0106,0.0430], \\ N_m \in [2,4], \\ D_m \in [12.1,16.8], \\ N_c \in [10,20], \\ D_c \in [0.5,1.5]. \end{cases} \tag{24}$$

Different from the optimal selection of the single objective optimization problem, the multi-objective optimization problem [18–20] involved in this paper contains two conflicting optimization objectives. It is difficult for the objective parameters combustion efficiency η and total pressure loss Δp to reach the optimal simultaneously. Therefore, in the optimization process, the two conflicting objectives can only be weighed to reach the Pareto optimal. Finally, an optimal solution set (i.e. Pareto solution set) containing multiple elements is obtained.

4 Experiments and analysis of the results

4.1 Analysis of combustion performance surrogate model based on POD-Hierarchical-Kriging

In this section, based on the model and method deduced above, the experimental process is mainly carried out to collect samples of combustion performance parameters of aero-engine combustor model, and the POD-Hierarchical-Kriging surrogate model is established for prediction. Firstly, based on 91 sets of sample data after Latin hypercube sampling and pre-processing, the one-dimensional procedure of the aero-engine combustion chamber model designed by Northwestern Polytechnical University is used to obtain the calculation results of the target optimization parameters corresponding to the sample data, and then the construction of the sample data set is completed.

After that, parameter estimation of the POD-Hierarchical-Kriging surrogate model is performed to obtain surrogate models of combustion efficiency η and total pressure loss Δp.

Using the above established model, 20 groups of untrained test data are used to test the prediction accuracy of the established surrogate model, and root mean square error (RMSE) is used as the measurement of error magnitude. The prediction errors of the model for combustion efficiency and total pressure loss are 0.0064% and 0.2523%,

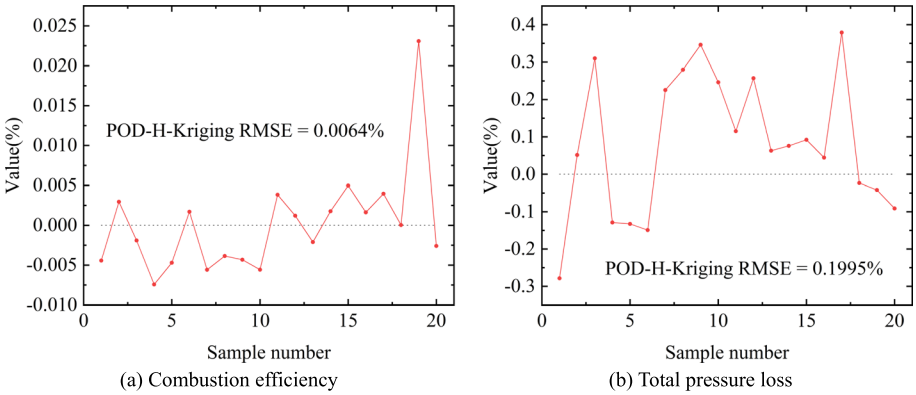

(a) Combustion efficiency (b) Total pressure loss

Fig. 6 Combustion efficiency prediction error

respectively. The relative prediction errors for the combustion efficiency and total pressure loss are shown in Fig. 6. We performed cross-validation of the POD-Hierarchical-Kriging model to calculate the fitness between the model and the flow solver. The results of the cross-validation of the predicted data points are depicted in Fig. 7. The horizontal axis represents the original values of the test data and the vertical axis represents the values predicted by the POD-Hierarchical-Kriging model. If the sample points are closer to the symmetrical diagonal, the model is considered accurate [21].

The accuracy of the POD-Hierarchical-Kriging model is preliminarily verified based on the prediction error relative graph and cross validation graph. In order to fully validate the advantages of the POD-Hierarchical-Kriging model as a prediction of combustion chamber performance, a comparison with other methods is necessary. The POD-Hierarchical-Kriging model is compared with the commonly used cubic polynomial response surface model, the basic Kriging model, and the Hierarchical-Kriging model. The basic Kriging model is trained using two schemes. The first scheme is trained with 91 sample points (Notated as A-Kriging model) and the second scheme is trained with only 12 high confidence samples (Notated as OH-Kriging model). The RMSE is used as the criterion to judge the prediction error of each model. The smaller the root mean square error of the model, the better the model prediction is.

As shown in Fig. 8, for the combustion efficiency, the RMSEs of the predictions of the four models using the new data set are 0.0115% for the cubic polynomial model, 0.018% for the A-Kriging model, 0.0128% for the OH-Kriging model, 0.0083% for the Hierarchical-Kriging model, and 0.0064% for the POD-Hierarchical-Kriging model. It is shown that all four surrogate models can well characterize the original model. For the combustion efficiency parameters, the POD-Hierarchical-Kriging model predicts the smallest RMSE, and the Hierarchical-Kriging model is the next best, both better than the cubic polynomial model and the basic Kriging model. Therefore, the POD-Hierarchical-Kriging surrogate model is accurate in predicting the combustion efficiency.

As shown in Fig. 9, for the total pressure loss, the RMSE of the predictions of the four models using 20 test data sets is 0.2002% for the cubic polynomial model, 0.1942% for the A-Kriging model, 0.4576% for the OH-Kriging model, 0.1833% for the Hierarchical-Kriging model, and 0.1995% for the POD-Hierarchical-Kriging model. It shows that the four surrogate models can well characterize the original model. However, for the total

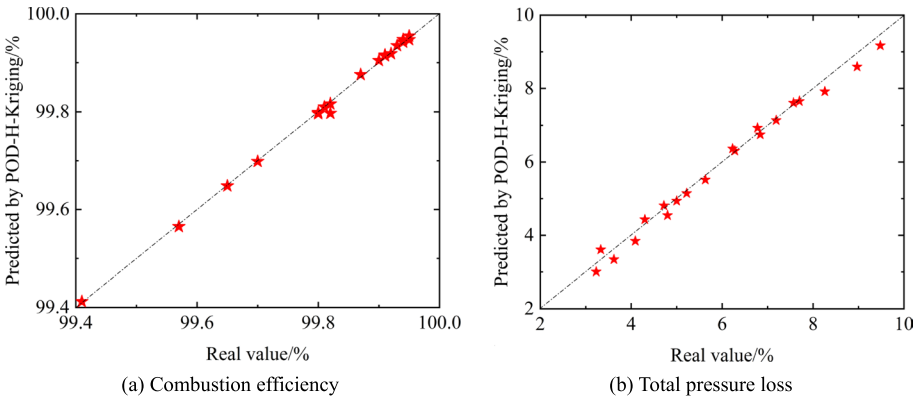

Fig. 7 Cross-validation data required for the POD-Hierarchical-Kriging model

pressure loss, the RMSE of the values predicted by the Hierarchical-Kriging model is the smallest. The POD-Hierarchical-Kriging model has similar predictions as the A-Kriging model. Their RMSEs are larger than those predicted by the Hierarchical-Kriging model and smaller than those of the cubic polynomial model. The RMSE of the OH-Kriging model is the largest, and its prediction is the worst.

By comparing with common surrogate models, the POD-Hierarchical-Kriging model shows its advantage as a model for predicting combustion chamber performance. Compared with the OH-Kriging model, the POD-Hierarchical-Kriging model performs better in both the prediction of combustion efficiency and the prediction of total pressure loss. This indicates that the POD-Hierarchical-Kriging model compensates for the problem that the basic Kriging model requires high confidence in the training sample points. It makes full use of the low confidence training samples in the sample dataset, thus improving the prediction accuracy. For comparison experiments on combustion efficiency prediction, the POD-Hierarchical-Kriging model has the best prediction effect and the RMSE of the POD-Hierarchical-Kriging model is 22.8% lower than the RMSE of the next best Hierarchical-Kriging model. It shows that the POD algorithm can better characterize the original data space, extract more critical sample information, and filter out marginal information after dimensionality reduction and reconstruction of the sample data set. For the prediction of total pressure loss, the prediction accuracy of the POD-Hierarchical-Kriging model is slightly lower than that of the optimal Hierarchical-Kriging model and higher than that of the cubic polynomial model. It is shown that combining the POD algorithm with the Hierarchical-Kriging model avoids overfitting and reduces computing loss to a certain extent. In the face of a large number of parameter predictions, the rapidity of the POD-Hierarchical-Kriging model can be demonstrated, and the prediction accuracy has not been greatly reduced.

4.2 Optimization results and analysis

Sensitivity analysis is used to study the influence of eight design variables on the two objective functions and to explore which decision variables have a greater or lesser influence on the test results. Figure 10 shows the sensitivity index analysis of design variables on combustion efficiency and total pressure loss respectively, as well as the influence

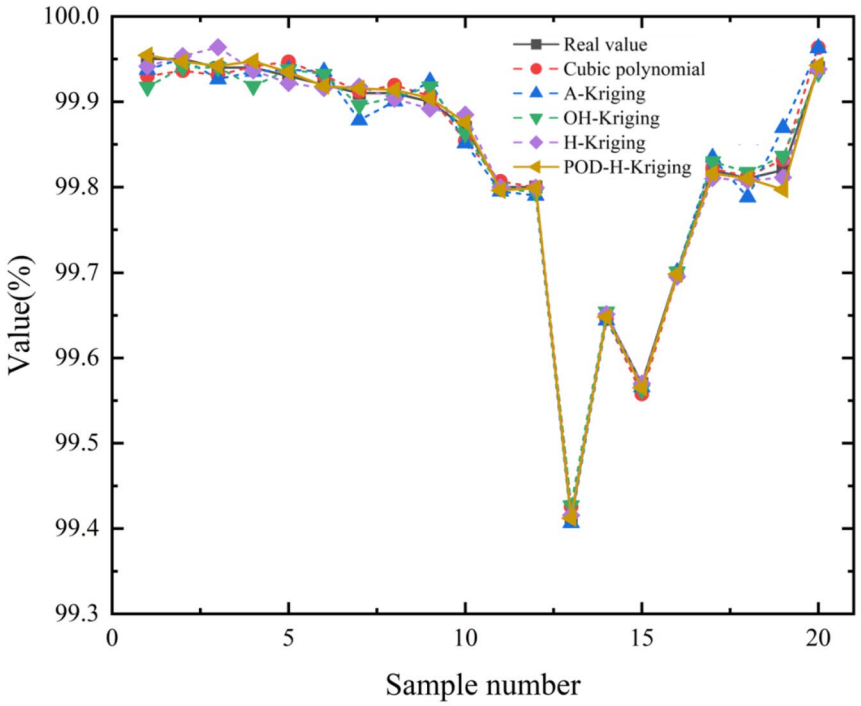

(a) Comparison of prediction results of various surrogate models on combustion efficiency

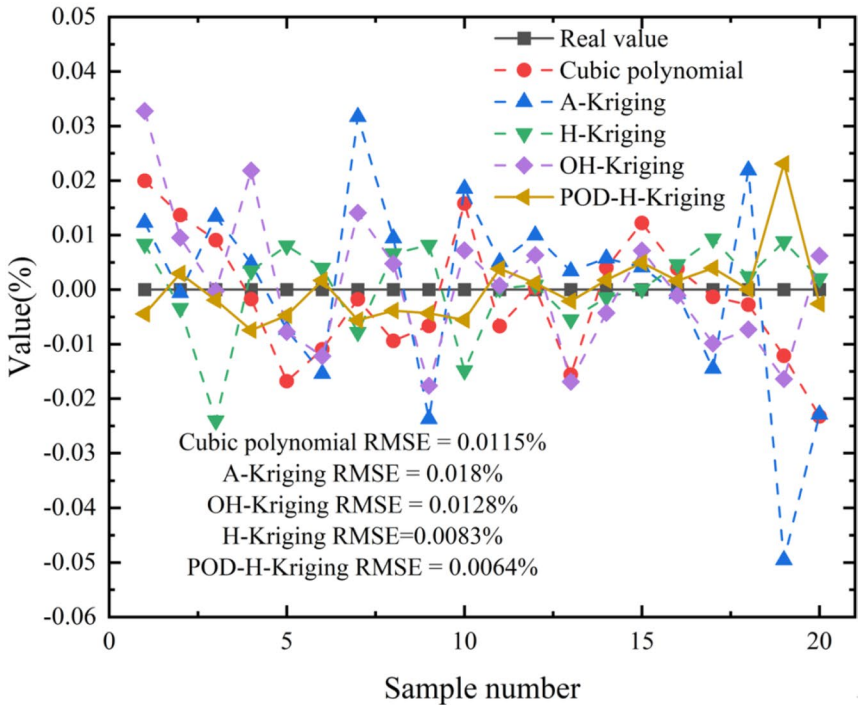

(b) Comparison of prediction errors of various surrogate models on combustion efficiency

Fig. 8 Comparison of predictions of surrogate models on combustion efficiency

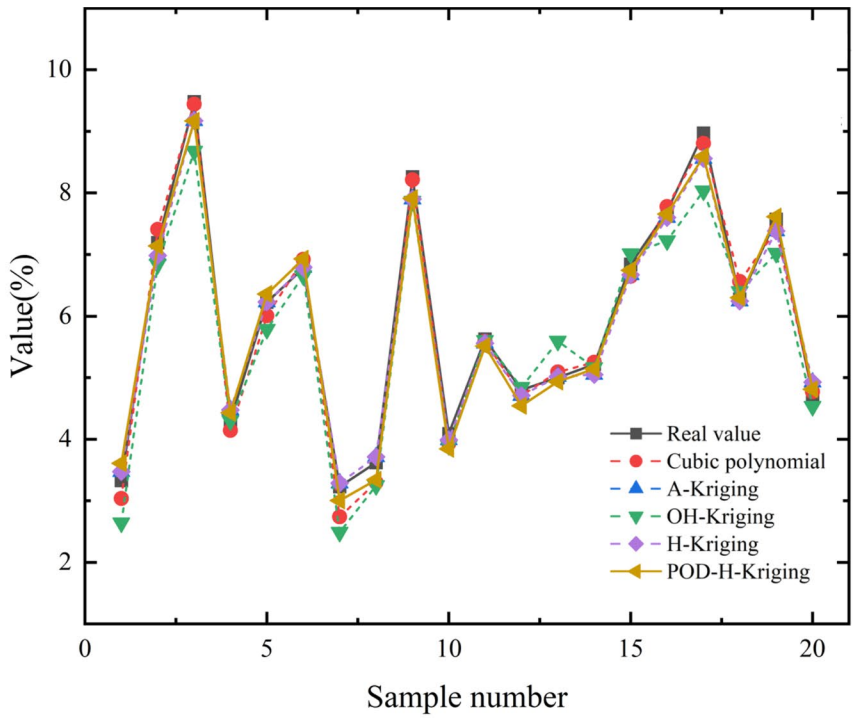

(a) Comparison of prediction results of various surrogate models on total pressure loss

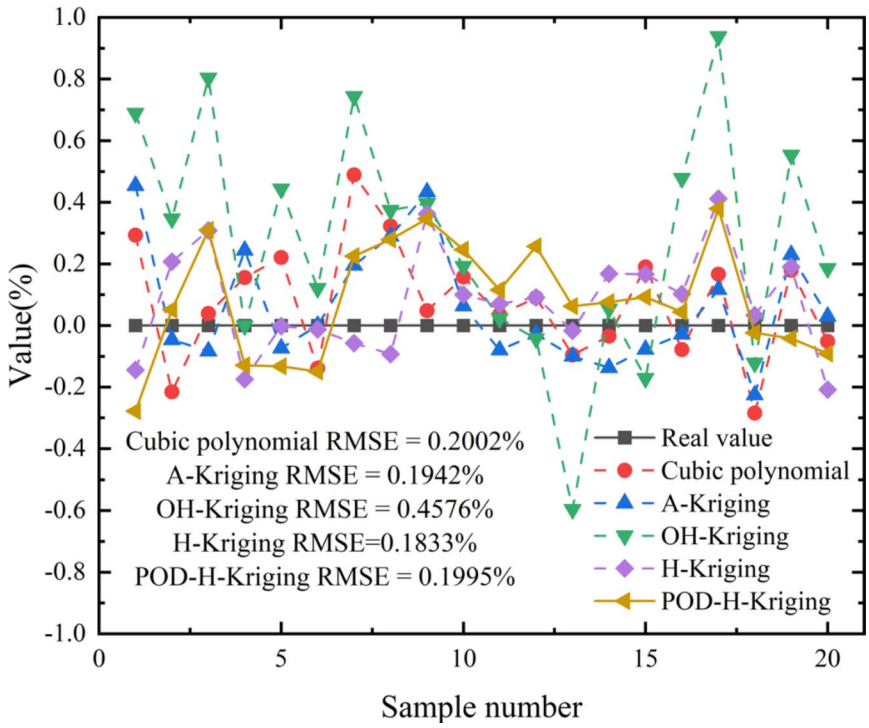

(b) Comparison of prediction errors of various surrogate models on total pressure loss

Fig. 9 Comparison of predictions of surrogate models on total pressure loss

ratio of each design variable. As shown in the figure, regardless of the sensitivity index of combustion efficiency or the sensitivity index of total pressure loss, the design variables with great influence are: total inlet temperature, total inlet pressure, total inlet flow and oil–gas ratio. The total influence of the other four design variables is less than 0.006% and can be ignored. Among them, the total inlet pressure has a great influence on the combustion efficiency and total pressure loss, so it can be seen that the design of total inlet pressure is in the dominant position in the combustion chamber design. In addition, the oil–gas ratio has the greatest influence on the combustion efficiency of the combustion chamber, and the total inlet flow has the greatest influence on the total pressure loss of the combustion chamber. Therefore, when optimizing the combustion chamber design, it is advisable to focus on the four aspects of total inlet temperature, total inlet pressure, total inlet flow and oil–gas ratio.

Based on the POD-Hierarchical-Kriging surrogate model, the optimization of aero-engine combustion chamber configuration parameters is carried out for the target optimization parameters of combustion efficiency η and total pressure loss Δp. The NSGA-II algorithm is used to solve the non-dominant solutions of two objective functions constructed by the POD-Hierarchical-Kriging surrogate model. The population size and iteration size are 200 and 50, respectively. The crossover rate and mutation rate are fixed at 1 and 0.03. Crossover parameters and mutation parameters are fixed at 100 and 100.

Pareto front is shown in Fig. 11. The horizontal and vertical axes are total pressure loss and combustion efficiency respectively. As shown in the figure, the overall trend of the Pareto solution set is that as the combustion efficiency increases, the total pressure loss also increases.

The constraint OTDF is predicted by using the basic Kriging surrogate model during the iterative process. Figure 12 illustrates the constraints to satisfy OTDF in the process of optimizing the two objective functions. The dotted line indicates the boundary of the design space, and the shaded area indicates the area outside the design constraints.

It can be seen from Fig. 12 that the Pareto fronts all meet the restriction of OTDF. It is also observed that most of the solutions in the optimal solution set have OTDFs greater than 0.1, indicating that most of the solutions in the Pareto solution set obtained by solving the multi-objective optimization of combustion efficiency and total pressure loss will have larger OTDFs. Based on the sensitivity analysis of combustion efficiency and total pressure loss, the influence of these design variables on combustion efficiency and total pressure loss is further explored by using the four design variables with great influence. According to the Pareto solution set of the POD-Hierarchical-Kriging model, the influence of the four variables on the two objective functions is shown in Figs. 13 and 14.

The relationship between total pressure loss and combustion efficiency with design variables is analyzed according to the four influential design variables using the Pareto solution set of the POD-Hierarchical-Kriging model. Figure 13a plots the relationship between the combustion efficiency and the total inlet temperature. Figure 13b plots the relationship between the combustion efficiency and the total inlet pressure. Figure 13c plots the relationship between the combustion efficiency and the total inlet flow. Figure 13d plots the relationship between the combustion efficiency and the oil–gas ratio. As shown in Fig. 13a, in the Pareto solution set, the combustion efficiency of the optimal

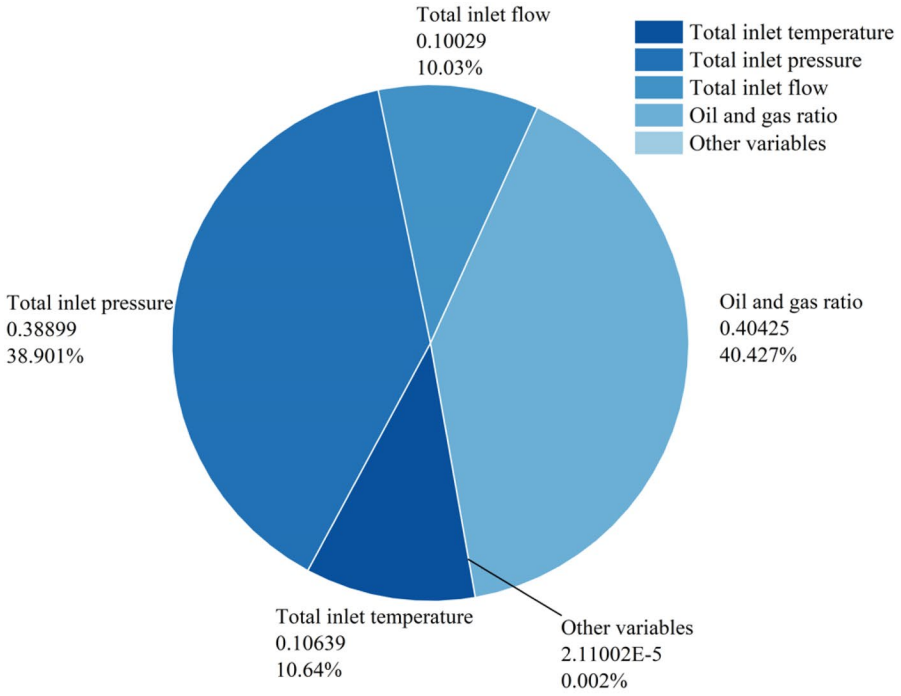

(a) Global sensitivity analysis of combustion efficiency

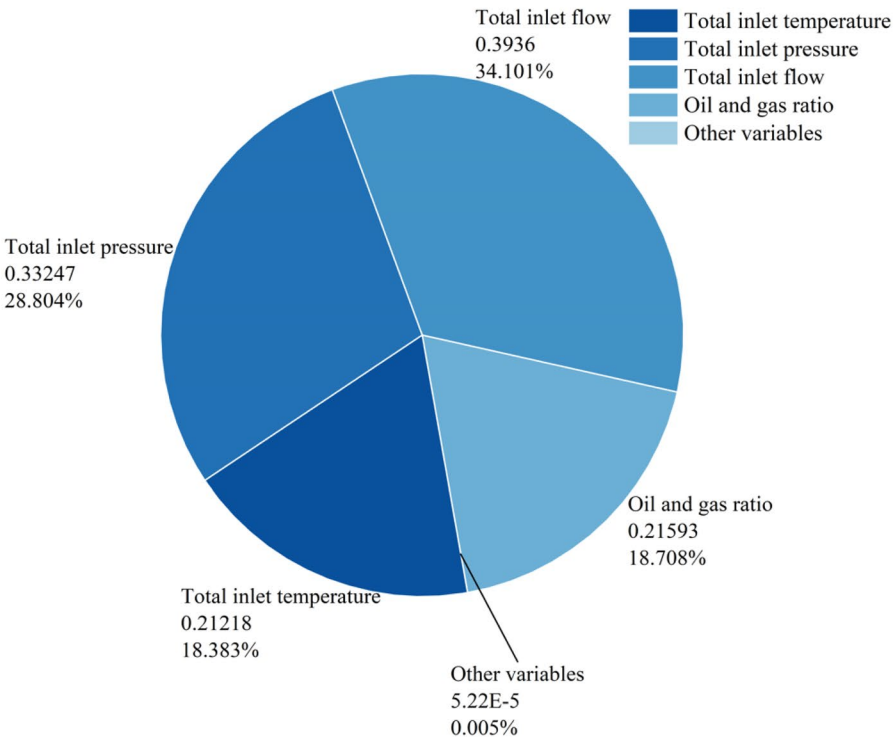

(b) Global sensitivity analysis of total pressure loss

Fig. 10 Global sensitivity analysis of combustion efficiency and total pressure loss

solution is small as the total inlet temperature is between 550 K and 650 K, and the combustion efficiency of the optimal solution is large as the total inlet temperature is between 650 K and 750 K. The iteration of the genetic algorithm produces a large number of individuals whose total inlet temperature is between 650 K and 750 K, indicating the superior property of the total inlet temperature between 650 K and 750 K in the design of the combustion chamber. As shown in Fig. 13b, the combustion efficiency of the optimal solution is relatively high as the total inlet pressure is between 2000 kPa and 3000 kPa, and the individuals tend to aggregate first and then disperse with the increase of the inlet total pressure. It reflects that increasing the total inlet pressure within a certain range will be beneficial for improving the combustion efficiency, while when the total inlet pressure is too large, the property of improving the combustion efficiency will be lost. As shown in Fig. 13c, two optimal solutions with the lowest combustion efficiency occur as the total inlet flow is between 40 kg/s and 45 kg/s. As for combustion efficiency, the design variable of total inlet flow in the whole population has no obvious aggregation, which confirms that the influence of total inlet flow on combustion efficiency is smaller than that of total inlet pressure and oil–gas ratio in sensitivity analysis. As shown in Fig. 13d, a large number of optimal solutions in the Pareto solution set are clustered as the oil–gas ratio is between 0.03 and 0.035, reflecting the excellent property of the oil–gas ratio between 0.03 to 0.035 on the combustion efficiency. After iteration, the oil–gas ratio between 0.025 and 0.035 shows a significant aggregation, which is consistent with the largest influence of oil–gas ratio on combustion efficiency in sensitivity analysis.

Figure 14a plots the relationship between the total pressure loss and the total inlet temperature. Figure 14b plots the relationship between the total pressure loss and the total inlet pressure. Figure 14c plots the relationship between the total pressure loss and the total inlet flow. Figure 14d plots the relationship between the total pressure loss and the oil–gas ratio. As shown in Fig. 14a, more optimal solutions with

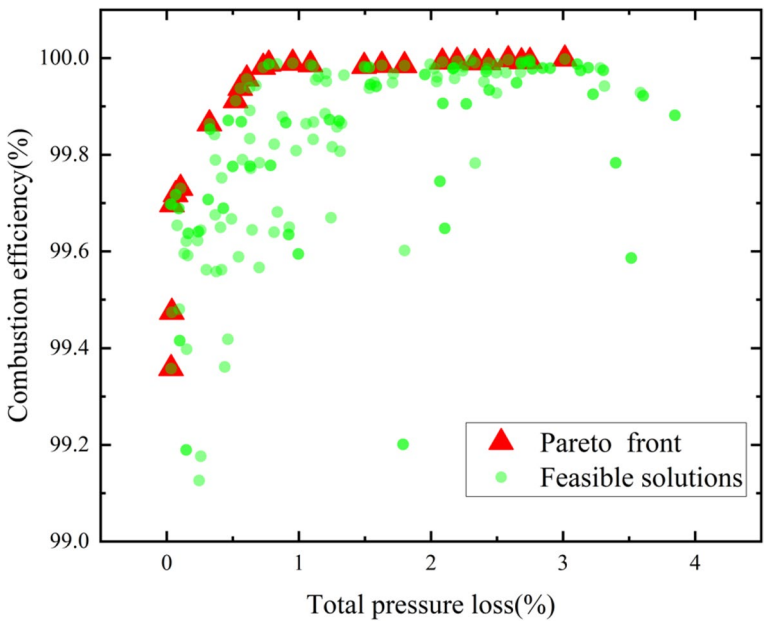

Fig. 11 Pareto front in the target space

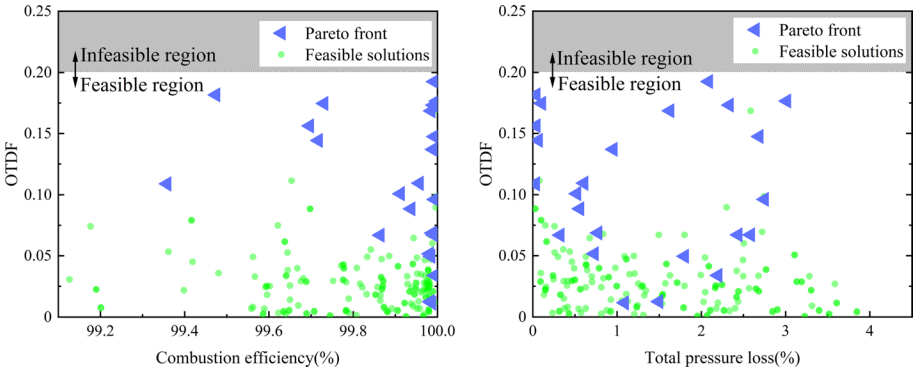

(a) Combustion efficiency and OTDF (b) Total pressure loss and OTDF

Fig. 12 OTDF constraint for optimal designs

low total pressure loss occur in the Pareto solution set as the total inlet temperature is between 550 K and 650 K, while more optimal solutions with high total pressure loss are obtained as the total inlet temperature is between 650 K and 750 K. This corresponds exactly to the influence of the total inlet temperature on the combustion efficiency in Fig. 13a, where the combustion efficiency is smaller for the optimal solutions as the total inlet temperature is between 550 K and 650 K and larger for the optimal solutions as the total inlet temperature is between 650 K and 750 K. It indicates that the total inlet temperature needs to be designed with a trade-off between high combustion efficiency and low total pressure loss in the optimization process with combustion efficiency and total pressure loss as the optimization objective. As shown in Fig. 14b, more optimal solutions with low total pressure loss occur as the total inlet pressure is between 1500 kPa and 2500 kPa. In Fig. 13b, the optimal solution has a larger combustion efficiency as the total inlet pressure is between 2000 kPa and 3000 kPa. It is inferred that the design variables in the combustion chamber design process will have better performance in the combustion chamber as the total inlet pressure is between 2000 kPa and 2500 kPa. As shown in Fig. 14c, many of the optimal solutions in the Pareto solution set aggregate as the total inlet flow is between 60 kg/s and 75 kg/s. As shown in Fig. 14d, aggregation occurs as the oil–gas ratio is between 0.03 to 0.035; however, many optimal solutions have total pressure loss greater than 1% as the oil–gas ratio is between 0.03 and 0.035. In the non-aggregated oil–gas ratio between 0.02 and 0.025, there are more optimal solutions with low total pressure loss. In Fig. 14d, the optimal solutions clustered have higher combustion efficiency as the oil–gas ration is between 0.03 and 0.035. It shows that the aggregation of individuals for the design variable of oil–gas ratio produced during the iterative process is mainly used to seek higher combustion efficiency. Therefore, the change in oil–gas ratio during the design of the combustion chamber will have a greater influence on the change in combustion efficiency. It corresponds to the fact that the oil–gas ratio has the greatest influence on the combustion efficiency during the sensitivity analysis, while the oil–gas ratio has less influence on the total pressure loss than the total inlet pressure and the total inlet flow.

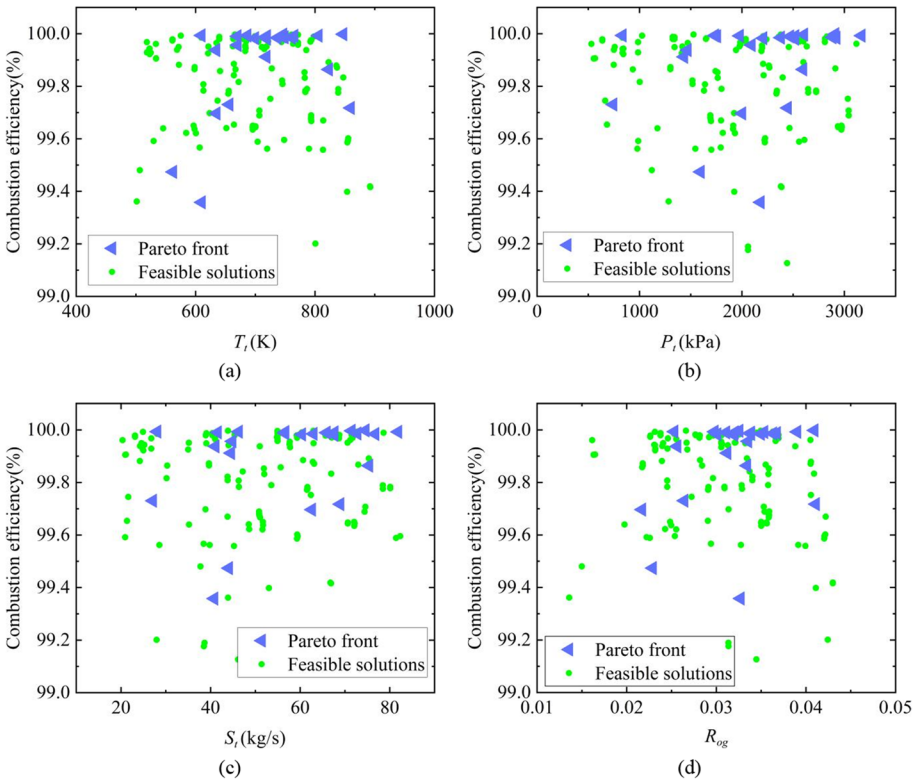

Fig. 13 Influence and variation of T_t, P_t, S_t and R_{og} on combustion efficiency

5 Conclusion

In view of the long calculation cycle, high processing test and cost of the traditional aero-engine combustion chamber design process, which restricts the engine optimization design cycle, this paper innovatively proposes a surrogate model for the performance of aero-engine combustion chambers based on the POD-Hierarchical-Kriging method. This work can be summarized as follows.

(1) Firstly, we apply a concentric graded combustion chamber of an aero-engine independently developed by Northwestern Polytechnical University, innovatively merge the POD algorithm with the Hierarchical-Kriging model, and propose a POD-Hierarchical-Kriging based combustion performance surrogate model method. The sample data are reconstructed by the POD method to reduce order, and then the design variables are performed by using the downscaled data. A study on the design and construction of a surrogate model for the performance of the combustion chamber is carried out. Through experiments, the predicted results of the POD-Hierarchical-Kriging model are compared and analyzed with the calculated results of the one-dimensional program, and the root mean square error of the predicted values of combustion efficiency and total pressure loss is 0.0064% and 0.1995%, respectively.

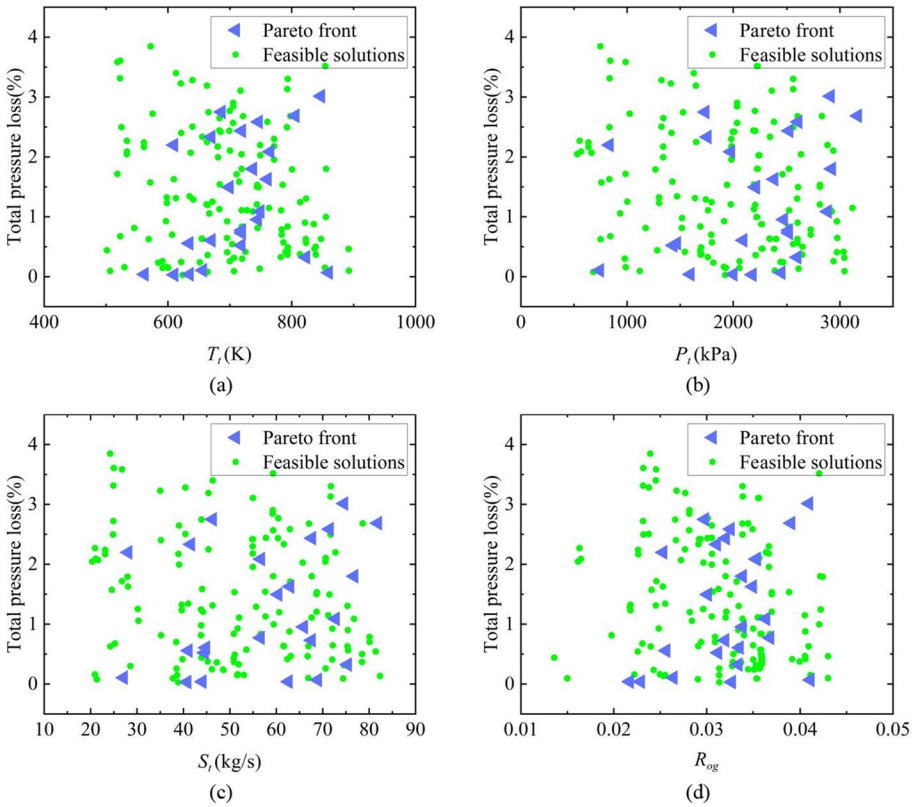

Fig. 14 Influence and variation of T_t, P_t, S_t and R_{og} on total pressure loss

(2) Subsequently, the POD-Hierarchical-Kriging model is compared with the cubic polynomial response surface model, the basic Kriging model and the Hierarchical-Kriging model. It is found that the POD-Hierarchical-Kriging model combines the advantages of the POD method and the Hierarchical-Kriging model. The POD-Hierarchical-Kriging model can better characterize the original data space, extract more critical sample information, and make full use of low confidence training sample points combined with a small number of high-precision training sample points to achieve high-precision prediction of unknown points. Compared with traditional simulations and numerical calculations, the POD-Hierarchical-Kriging model has a faster prediction speed.

(3) On this basis, the multi-objective NSGA-II optimization method is applied to further carry out a parametric optimization study on eight design variables. Under the constraints, high combustion efficiency and low total pressure loss are the optimization objectives. Through sensitivity analysis, it is known that the design variables of total inlet temperature, total inlet pressure, total inlet flow and oil–gas ratio have a greater influence on the combustion efficiency and total pressure loss. Among them, the oil–gas ratio has the greatest influence on the combustion efficiency, and the total inlet flow has the greatest influence on the total pressure loss. A Pareto solution set is obtained by the NSGA-II optimization method. By analyzing

the Pareto solution set, the NSGA-II multi-objective optimization results based on the POD-Hierarchical-Kriging surrogate model can correspond to sensitivity analysis. The critical design factors and the specific influence states of the design parameters on the target parameters that have a large impact on the design objectives are obtained to guide the optimal design of the combustion chamber.

Acknowledgements
Not applicable.

Authors' contributions
JL and HZ conceptualized the idea, while MG and HW proposed the methods used in the study. ST and YM carried out simulations, while WS was responsible for data acquisition. ST wrote the draft of the manuscript, while YT reviewed and edited it. YT also implemented the revision of the manuscript together with MG. All authors read and approved the final manuscript.

Funding
This project was supported by Sichuan Science and Technology Program (Grant No. 2023YFG0336).

Availability of data and materials
The data that support the findings of this study are available from the corresponding author upon reasonable request.

Declarations

Competing interests
The authors declare that there are no conflicts of interest regarding the publication of this paper.

Received: 6 February 2023 Accepted: 17 April 2023
Published online: 03 July 2023

References

1. Zhang X, Zhao YG, Yang C (2023) Recent developments in thermal characteristics of surface dielectric barrier discharge plasma actuators driven by sinusoidal high-voltage power. Chin J Aeronaut 36(1):1–21
2. Taghavi M, Gharehghani A, Nejad FB et al (2019) Developing a model to predict the start of combustion in HCCI engine using ANN-GA approach. Energy Convers Manag 195:57–69
3. Poggi C, Rossetti M, Bernardini G et al (2022) Surrogate models for predicting noise emission and aerodynamic performance of propellers. Aerosp Sci Technol 125:107016
4. Ogawa H (2015) Physical insight into fuel-air mixing for upstream-fuel-injected scramjets via multi-objective design optimization. J Propul Power 31(6):1505–1523
5. Tejero F, MacManus DG, Sheaf C (2019) Surrogate-based aerodynamic optimisation of compact nacelle aero-engines. Aerosp Sci Technol 93:105207
6. Tejero F, Christie R, MacManus D et al (2021) Non-axisymmetric aero-engine nacelle design by surrogate-based methods. Aerosp Sci Technol 117:106890
7. Han ZH, Görtz S (2012) Hierarchical kriging model for variable-fidelity surrogate modeling. AIAA J 50(9):1885–1896
8. Du D, He E, Li F et al (2020) Using the hierarchical Kriging model to optimize the structural dynamics of rocket engines. Aerosp Sci Technol 107:106248
9. Yang M, Tian Y, Guo M et al (2023) Optimized design of aero-engine high temperature rise combustion chamber based on "kriging-NSGA-II." J Braz Soc Mech Sci Eng 45(1):59
10. Ma Y, Tian Y, Le J et al (2023) High-dimensional multiobjective optimization of an aeroengine combustor based on cubic polynomial. J Aerosp Eng 36(2):04022124
11. Liu C, Zhong H, Song W et al (2019) Simulation analysis and optimization on test method of combustor airflow distribution. J Aerosp Power 34(8):1652–1662
12. Xiong S, Song W, Mei Y (2021) Study on one-dimensional calculation method of aero-engine combustion chamber. In: Proceedings of the fifth symposium on ramjet coupled internal and external flow, Shandong University, Weihai, 22-25 July 2021. pp 745–755
13. De Cillis G, Cherubini S, Semeraro O et al (2020) POD analysis of the recovery process in wind turbine wakes. J Phys Conf Ser 1618(6):062016
14. Kean K, Schneier M (2020) Error analysis of supremizer pressure recovery for POD based reduced-order models of the time-dependent Navier-Stokes equations. SIAM J Numer Anal 58(4):2235–2264
15. De Cillis G, Cherubini S, Semeraro O et al (2021) POD-based analysis of a wind turbine wake under the influence of tower and nacelle. Wind Energy 24(6):609–633
16. Martin JD, Simpson TW (2005) Use of kriging models to approximate deterministic computer models. AIAA J 43(4):853–863
17. Aygun H, Turan O (2022) Application of genetic algorithm in exergy and sustainability: a case of aero-gas turbine engine at cruise phase. Energy 238:121644

18. Abdallah I, Lataniotis C, Sudret B (2019) Parametric hierarchical kriging for multi-fidelity aero-servo-elastic simulators—application to extreme loads on wind turbines. Probab Eng Mech 55:67–77
19. Ren T, Zhu ZL, Dimirovski GM et al (2014) A new pipe routing method for aero-engines based on genetic algorithm. Proc Inst Mech Eng Part G J Aerosp Eng 228(3):424–434
20. Rogero JM (2002) A genetic algorithms based optimisation tool for the preliminary design of gas turbine combustors. Dissertation, Cranfield University
21. Lee S, Yee K, Rhee DH (2017) Optimization of the array of film-cooling holes on a high-pressure turbine nozzle. J Propul Power 33(1):234–247

Publisher's Note